Effect of rubber reactivity on the morphology of polybenzoxazine blends investigated by atomic force microscopy and dynamic mechanical analysis

ARTICLE *in* JOURNAL OF APPLIED POLYMER SCIENCE · MAY 2006

Impact Factor: 1.77 · DOI: 10.1002/app.23430

3 AUTHORS, INCLUDING:

Hatsuo Ishida
Case Western Reserve University
448 PUBLICATIONS **12,896** CITATIONS

SEE PROFILE

Effect of Rubber Reactivity on the Morphology of Polybenzoxazine Blends Investigated by Atomic Force Microscopy and Dynamic Mechanical Analysis

Yu-Hsin Lee, Douglas J. Allen, Hatsuo Ishida

Department of Macromolecular Science and Engineering, Case Western Reserve University, Cleveland, Ohio 44106-7202

Received 8 July 2005; accepted 18 August 2005
DOI 10.1002/app.23430
Published online in Wiley InterScience (www.interscience.wiley.com).

ABSTRACT: Atomic force microscopy (AFM) is employed to study the hydroxyl-terminated polybutadiene (HTBD) rubber-modified polybenzoxazine resin. The morphology exhibits a submicron phase separation when HTBD with low epoxy contents are used. No distinguishable phase separation appears in the blend modified with high epoxy content HTBD. The rubber and resin phases are identified by the change of nanoscale indentation as a function of external load imposed on the cantilever. The existence of an interphase between the glassy matrix and the rubbery domain is shown by comparing the pulling distances from force–distance (F–d) curve measurements. The extent of rubber cavitation is investigated by the particle analysis on the fracture surface and is found to increase with the particle diameter. The amount of dissolved rubber, estimated by the Fox equation, increases with the rubber reactivity, and the data corroborates well with the observed morphology. © 2006 Wiley Periodicals, Inc. J Appl Polym Sci 100: 2443–2454, 2006

Key words: cavitation; dynamic mechanical analysis (DMA); force–distance curve; lateral force microscopy (LFM); reactive rubber

INTRODUCTION

The addition of a low T_g phase is often used to enhance the fracture toughness of a glassy polymer. To prevent from significantly compromising the desirable properties by a soft inclusion, the interphase between these two distinct components needs to be optimized by means of physical or chemical bonding. Successful application of this technique to overcome the brittleness of polybenzoxazine resins was first attempted by adding engineering plastics such as poly(ε-caprolactone) (PCL),[1] although brittleness is not necessarily an inherent property of polybenzoxazine. The observed 50% improved fracture strength in the blend with 13 wt % of PCL is attributed to hydrogen bonding formation upon curing.[1] The incorporation of reactive rubber has also been demonstrated to toughen polybenzoxazine resins without undue sacrifices to the desirable properties.[2] The functional groups serve to minimize the surface tension between the matrix and the rubbery domains,[3] and the apparent low viscosity can facilitate the mixing prior to curing. Hydroxyl-terminated polybutadiene (HTBD) rubber with various epoxy contents was selected as the toughening modifier, as the epoxidized polybutadiene rubber can undergo a copolymerization with the hydroxyl groups produced upon benzoxazine ring opening and thus can be chemically grafted into the matrix network.[4] Hence, a toughener with a higher compatibility with the polybenzoxazine matrix is anticipated. Furthermore, with various epoxy weight fractions on the rubber, the effect of rubber reactivity on the blend morphology can be systematically evaluated.

Rubber modification has been found to be a very successful approach to overcome the inherent brittleness of thermosets.[5,6] Cavitation of rubber particles, followed by plastic deformation of the matrix, is believed to be the major toughening mechanism.[7–9] Researchers agree that cavitation alone is not a considerable source of toughening, yet its importance on the plastic deformation of the matrix has been widely recognized.[10,11] The plastic deformation, which is induced by rubber particles, can be categorized into two mechanisms: one is shear yielding of matrix between the neighboring rubber particles and the other is plastic void growth of the matrix surrounding the particle.[10] It is also identified that the role of the rubber particles in the matrix phase is to relieve the constraint in front of crack tips by rubber cavitation,[12] which thereby triggers the formation of shear bands.[10] Various morphological parameters, such as particle size, particle size distribution, and matrix-to-particle adhesion, play an important role in toughening.[11,13–15]

Correspondence to: H. Ishida (hxi3@case.edu).

TABLE I
Physical Properties of the Reactive Hydroxyl-Terminated Polybutadiene (HTBD) Rubbers with Low Epoxy (LEBD) and High Epoxy Content (HEBD) used to Toughen Polybenzoxazine

Type of rubber	Oxirane oxygen (wt %)	Viscosity (MPa s)	Solubility parameter ($MPa^{1/2}$)	Molecular weight (M_n; 10^3g/mol)	Polydispersity	Specific gravity (g/cm^3)	T_g (°C)
HTBD	0	1500	17.2	2.8	2.3	0.90	−75
LEBD	3.5	5500	17.7	2.9	2.4	1.01	−60
HEBD	6.1	23000	18.2	3.3	2.8	1.01	−47

Most research in this area has concentrated on the relationships between the morphology and the physical properties of rubber-toughened thermosets. Comparatively little has been done to investigate the properties of the rubber particles themselves, although they are a critical part of the toughening. Accordingly, this article attempts to interpret the degree of rubber cavitation on the basis of blend morphology of the resin that is being modified by rubbers with different reactivity. Four major goals of our study were (i) to use AFM to examine the morphology variation when three different types of rubber tougheners are being used; (ii) to use F–d measurements to identify two blend components; (iii) to present the close relationship between the particle diameter and the cavity depth; and (iv) to review the correlation between bulk viscoelastic properties and fractured surface properties probed by AFM.

EXPERIMENTAL

Sample preparation

The rubber modifiers used in this study are three different grades of hydroxyl-terminated poly(butadiene) (HTBD) supplied by the Elf-Atochem Company (France). The internal oxirane ring (epoxy) present on the butadiene rubber backbone is obtained by reaction of cis and trans unsaturations with an organic peracid. HTBD rubber with low and high epoxy content is abbreviated as LEBD and HEBD throughout this communication for simplicity, and HTBD is used specifically for the rubber without any epoxy content. The detailed physical properties of these rubber modifiers are listed in Table I. The polybenzoxazine monomer was synthesized through the Mannich reaction of stoichiometric quantities (2 : 4 : 1) of phenol, paraformaldehyde, and 1,12-diaminododecane refluxed in chloroform for 12 h at a concentration of 5 mL solvent/g of reactant. Chemicals with purities greater than 95% were purchased from Sigma–Aldrich Chemical Company and used without further purification. The monomer solution was then washed with 1*N*-sodium hydroxide solution, rinsed until neutral, and dried over sodium sulfate. Chloroform was removed by rotary evaporation, and the monomer was refrigerated until use. A detailed description of the synthesis and purification procedure is presented elsewhere.[16] The chemical structures of the benzoxazine prior to and after curing are displayed in Scheme 1.

Rubber-modified polybenzoxazine samples were prepared by melt mixing 10 wt % of the polybutadiene rubber with benzoxazine monomer in an aluminum dish at 100°C. The clear homogeneous mixture was then poured into a vertical mold consisting of two surface-treated glass plates separated by a silicon rubber spacer. The resin-filled mold was then evacuated for 2 h at 100°C, followed by a step cure at temperatures of 145, 165, and 180°C, for 2 h at each step. All samples were cured without adding any catalyst or initiator, and care was taken to ensure that all cured samples were free of voids. After the completion of curing, the oven was turned off, allowing the samples to cool slowly to room temperature.

Instrument

AFM analyses were carried out with an Explorer (ThermoMicroscope, Sunnyvale, CA) in air. AFM contact probes (#1525) with a spring constant equal to

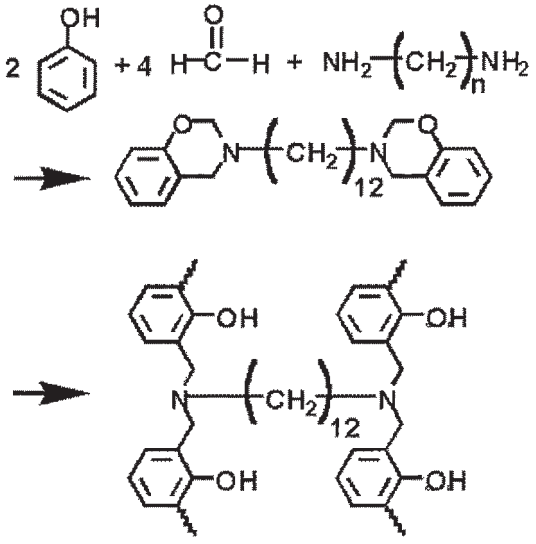

Scheme 1 Synthesis route to benzoxazine monomer preparation and the ring-opened polybenzoxazine resin.

0.032 N/m were used. This type of cantilever was fabricated from silicon nitride (Si_3N_4) and designed in a V-shape with a probe tip integrated onto the underside of the cantilever. The length, width, and thickness of the arm are 200, 18, and 0.6 μm, respectively, and the apex radius of the attached tip is about 20 nm according to the manufacture.

Lateral force microcopy

Lateral force microcopy (LFM) measures the lateral deflections of the cantilever. The direct output of the photodetector corresponding to the torsional movement of the cantilever, in units of nanoampere, is the photo-induced current, which was directly used to construct the images. The principle of LFM has been explicitly described in earlier works.[17–21]

Force–distance curve

F–d measurements are performed on preselected images where a well-defined spherical rubbery domain and continuous matrix phase can be seen. To identify these two phases, two sets of F–d curves were collected on the matrix and the rubber, respectively. Indent stiffness of these two phases in units of nN/nm, computed by dividing the applied force with the indentation depth, can be used to describe the "spring constant" of the material.[22]

Data analysis

Histograms of particle diameter (D) and rubber cavity depth (d) distribution were constructed from at least 100 particles among more than 20 images scanned from a fractured sample. The acquired topographic images were quantitatively examined by the "line analysis" mode of the software (SPM Lab, Version 5.0, ThermoMicroscope, CA). An approach to quantify the degree of rubber cavitation is illustrated in Scheme 2. The depth of the cavity (d) can be obtained from the height variation (z-signal) in the topographic images and is normalized over the radius of the spherical domains (R) estimated from both the x- and y-signal in the topographic image. It should be noted that the diameter was taken as the average value of x- and y-signal collected from each domain, and only the nearly perfect spherical domains with a diameter determined from x- and y-signal yielding less than 1% difference were used for analysis. This preselection of the perfectly spherical-shaped rubber would ensure the validity of the critical assumption upon which this methodology is built.

The normalized cavity depth (d/R) is an index proposed to describe the extent of internal rubber cavitation after the sample surface is fractured. A normalized cavity depth equal to 0 ($d/R = 0$) describes a completely filled cavity, while a normalized cavity depth equal to 1 ($d/R = 1$) would indicate an empty cavity, which implies a complete rubber debonding. Accordingly, domains with d/R close to 1, would suggest a more severe rubber cavitation upon fracture. Number–average ($\bar{D}_N$) and weight–average particle diameter ($\bar{D}_W$) can be derived from the equations listed here:

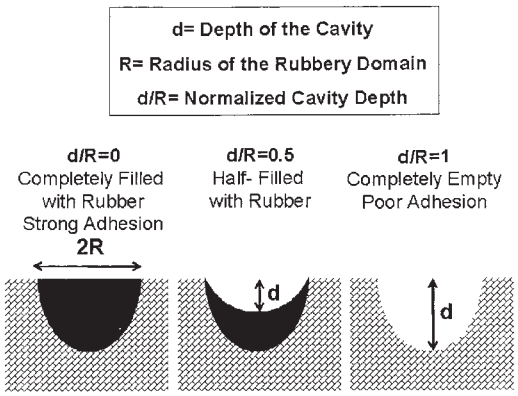

Scheme 2 Approach to quantify the depth of the cavity and an illustration to show the relationship between the amount of filled rubber and the normalized depth of cavity.

$$\bar{D}_N = \frac{\sum n_i D_i}{\sum n_i} \tag{1}$$

$$\bar{D}_W = \frac{\sum n_i D_i^2}{\sum n_i D_i} \tag{2}$$

Number and weight average normalized cavity depth, $(d/R)_N$ and $(d/R)_W$, can also be estimated in a similar fashion by the equations summarized here:

$$\left(\frac{d}{R}\right)N = \frac{\sum n_i (d/R)_1}{\sum n_1} \tag{3}$$

$$\left(\frac{d}{R}\right)W = \frac{\sum n_1 (d/R)_1^2}{\sum n_1 (d/R)_1} \tag{4}$$

Dynamic mechanical analysis

The rubber-modified polybenzoxazines were characterized in a Rheometrics Dynamic Mechanical Spectrometer (RMS-800) over the temperature range from -150 to 200°C at a heating rate of ~2°C/min. The strain chosen was 0.1%, which was shown by a strain sweep to be within the range of linear viscoelasticity for the materials while affording reasonable torque responses throughout the temperature range.[23] A typical frequency of 6.28 rad/s (1 Hz) was used in this study. Rectangular bars with an average size of 60 ×3

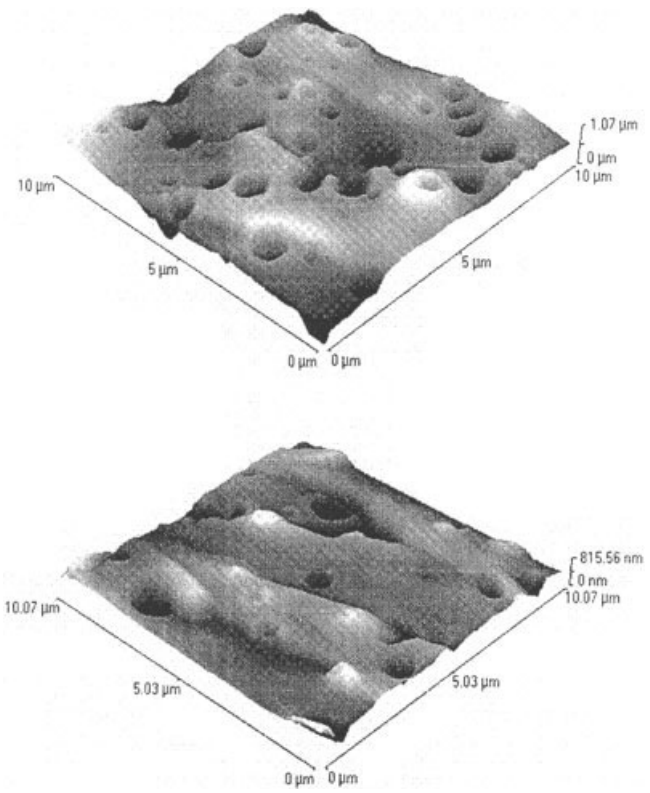

Figure 1 AFM topography images of polybenzoxazine blend with 10 wt % of HTBD rubber. Top (a) and bottom (b) represent sample prepared by fracture method and microtome, respectively.

$\times 12$ mm^3 were analyzed by a dual range force rebalance transducer set for the 2000 g cm torque range with a rectangular sample torsion fixture.

RESULTS AND DISCUSSION

Sample preparation

Displayed in Figure 1 are topographic images acquired from polybenzoxazine resins blended with 10 wt % of HTBD rubber. Figure 1(a) reveals the sample that was fractured at ambient temperature, and Figure 1(b) shows the surface created by a microtome sectioning. The fractured surface appears to have a greater number of rubber cavities and more detailed surface features than does the microtomed sample. This can easily be explained by the fact that when the sample was being microtomed, the surface plane was determined solely by the cutting knife. A smoother overall fracture surface would therefore be expected. However, when the surface was created by the fracture process, fracture lines would reveal where the actual mechanical deformation of the sample occurred. The deformation took place through routes where larger rubbery domains were located and it attempted to "find" the closest rubber ball to continue the route. As a result, a rougher surface and a greater number of spherical domains were revealed. In addition to the finer features, the former image may also provide information regarding morphology changes during fracture, allowing for a "real-time" fracture mechanism to be proposed based upon image analysis of those samples. Large rubbery domains serve as crack initiators, triggering the crack front to propagate along the equator of the spherical domain where the maximum stress is localized; thus, a much rougher surface and a greater number of dispersed phases would be visualized.[5] As a more vivid morphology was disclosed from the fracture sample, the systematic investigation throughout this article was only performed on samples prepared by this method.

Evidence of ductile failure

Shown in Figures 2(a) and 2(b) are the LFM forward and backward images of the resin blended with 10 wt

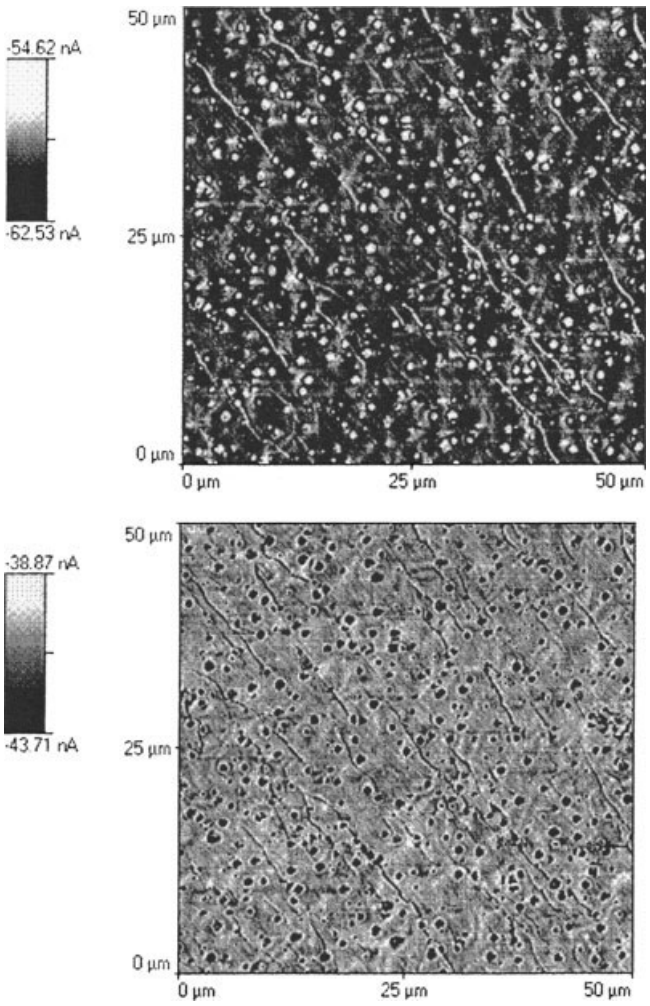

Figure 2 AFM images of polybenzoxazine blend with 10 wt % of HTBD rubber. Top (a) and bottom (b) represent LFM forward and LFM reverse images, respectively.

% HTBD rubber. Two interesting surface features, signifying a ductile failure in this scanning area of 50 by 50 μm^2, are discussed as follows. First, in addition to numerous and nearly perfect spherical domains, furrows running at angles of ~45 degree to the principle tensile stress (i.e., in the direction of maximum shear stress) are also visible, which can be classified as localized plastic shear bands.[5] Second, propagation of fracture fronts in the form of steady tear lines were initiated at large rubbery domains and terminated at small particles. It should be mentioned that the stress whitening, which can be observed by naked eyes in the failed samples, also suggests the occurrence of plastic flow, possibly in the form of crazing, which has been reported before.[24] Rubber particles blunt the sharp crack tip and disperse the stress concentrated on the equator of the rubber particle in various directions.[12] The toughening mechanism associated with this type of ductile sample suggests that both internal rubber cavitation and debonding can induce further shear yielding in the adjacent matrix phase and keep the shear forces localized, thereby delaying catastrophic failure.[5,8,9,12]

Effect of rubber reactivity on blend morphology

The bulk T_g of the polybenzoxazine used, as determined by dynamic mechanical analysis (DMA), is above room temperature (114°C), whereas that of HTBD is below room temperature (−75°C), as summarized in Table I**.** Thus, it is expected that the glassy polybenzoxazine and the rubbery HTBD phases can be distinguished fairly well even at the surface by topographic observation. With such a great difference in polymer chain mobility between the two phases, it is anticipated that LFM can exhibit a significant variation. An example of a topographic image of the blend with 10 wt % of HTBD rubber is shown in Figure 3(a)**.** Darker areas represent valleys and brighter areas are hills. Several spherical cavities are noticed in this 20 by 20 μm^2 scanning area. Differences in friction between the rubbery domains and the matrix can be clearly observed in the LFM images [Figs. 3(b) and 3(c)]**.** In the forward image scanned from the left to the right, the dark areas represent regions of low friction, while the bright areas represent regions of high friction. The opposite is true for the reverse images acquired from the right to the left. The discrete domains with a higher imposing torsion or greater LFM signal are rubber-enriched regions.

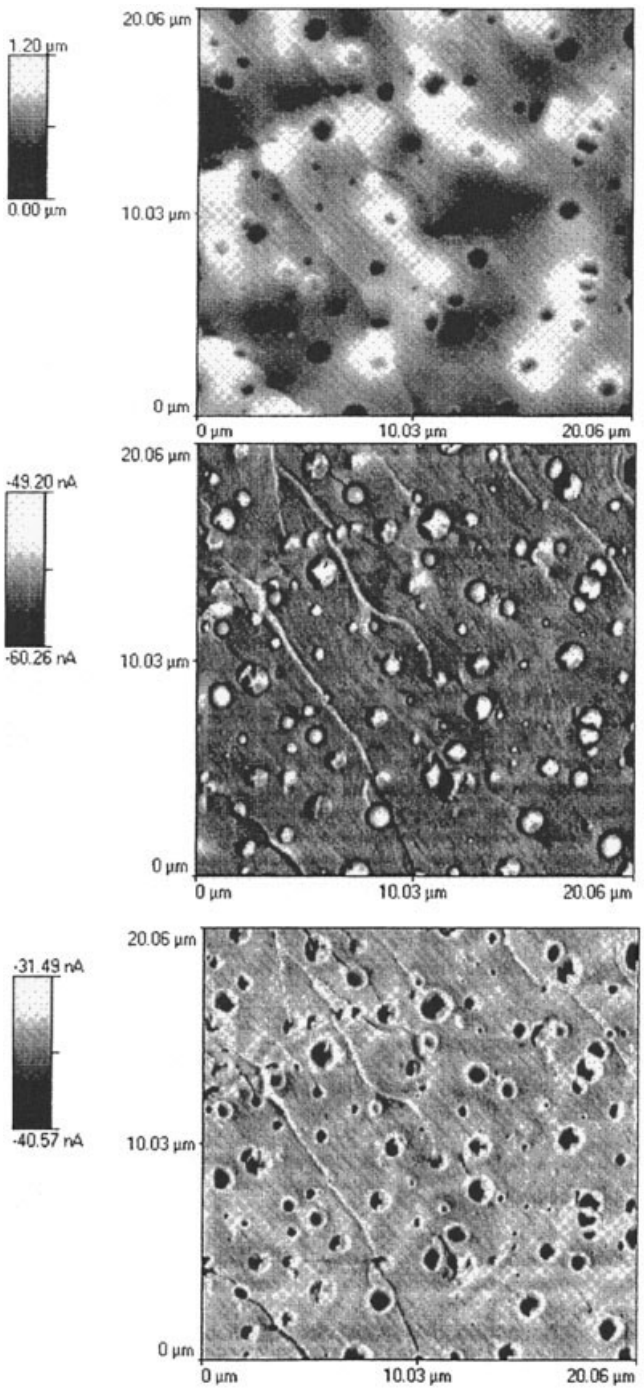

Figure 3 AFM images of polybenzoxazine blend with 10 wt % of HTBD rubber. Top (a) to bottom (c) represent topography, LFM forward, and LFM reverse images, respectively.

Topographic images of resins blended with HTBD rubbers of a low and high epoxy content are shown in Figures 4 and 5, respectively. Large and small scanning areas are both presented for a clearer view. A much smaller cavity size was found in the blend with LEBD rubber in comparison with the blend with HTBD rubber. No distinguishable morphology variation was observed in the blend with HEBD. The copolymerization reaction between epoxy and benzoxazine monomer during thermal curing has been reported by early researchers.[4] Thus, it is anticipated that the incorporation of epoxy from the rubber can significantly improve the compatibility between the toughener and the matrix resin. The higher the epoxy

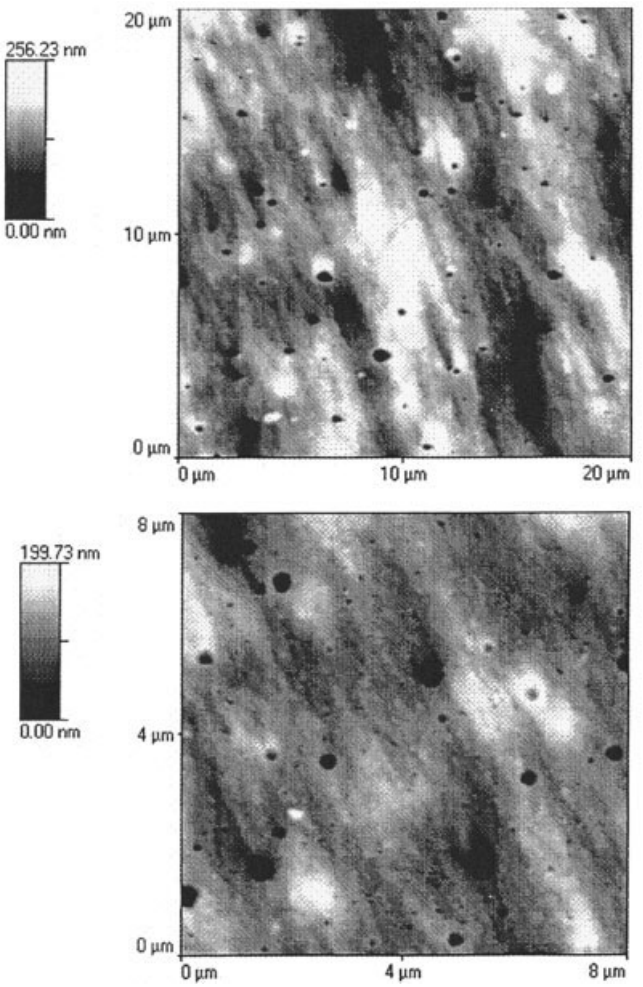

Figure 4 AFM images of polybenzoxazine blend with 10 wt % of LEBD rubber. Top (a) and bottom (b) represent topography in large and small scanning area, respectively.

contents in the rubber toughener, the greater the compatibility. As a result, smaller phase-separated rubbery domains would appear. The fracture surface of the highly compatibilized sample was clear, rather smooth, and monotonous, as seen in Figure 5, which resembles a brittle fracture mechanism.

Fracture surface analysis and sample appearance

It is generally regarded that roughness of the fracture sample provides a wealth of information on the extent of plastic deformation and can be adopted to correlate with the bulk mechanical performance. Therefore, it is of great significance to collect surface statistics, such as average height and roughness, from the topographic images of a fracture surface. The results are summarized in Table II. The pronounced rough morphology in the HTBD sample can be attributed to both multiple crack initiating sites, which occur at fairly large spherical domains,[12] and the subsequent shear yielding in the continuous phase. HEBD and LEBD rubber were much more finely and evenly distributed over the matrix phase than was HTBD owing to the chemical bonding that occurred during polymerization.

The sample appearance can also be associated with the size of the phase separation. The HEBD sample exhibits a complete transparency, which can be attributed to the clear topographic data bearing no distinguishable features as seen in Figure 5**.** The LEBD sample is translucent, which can be correlated with the fact that the spherical domains have a size approximately the wavelength of the visible light. The resin modified with HTBD appears to be completely opaque, owing to the existence of the large segregated domains.

Identification of two phases by f–d curves

As some of the dispersed domains appear to be cavities, an additional identification of the phases needs to

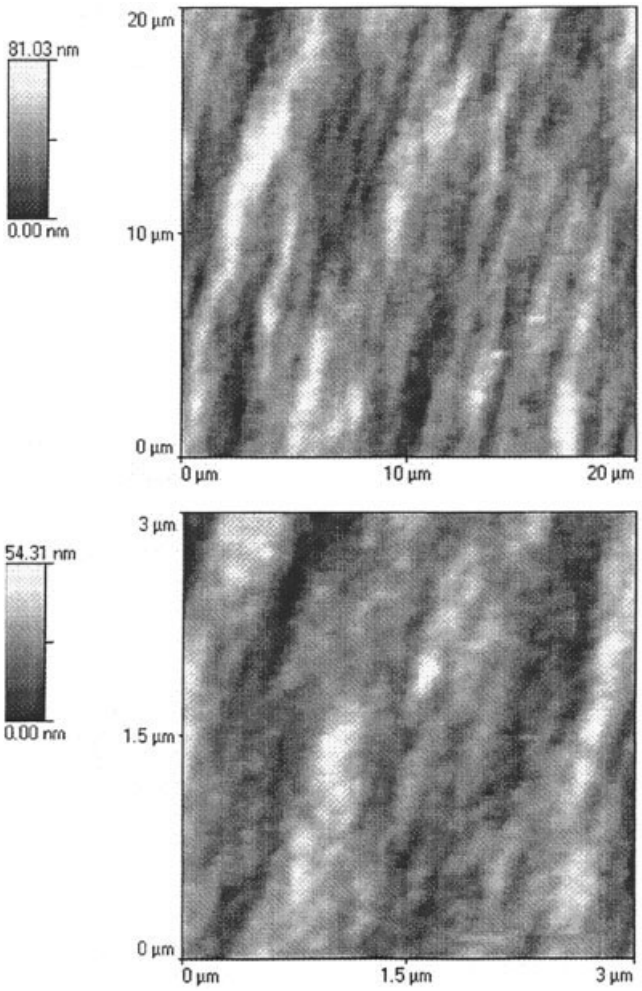

Figure 5 AFM images of polybenzoxazine blend with 10 wt % of HEBD rubber. Top (a) and bottom (b) represent topography image with a large and small scanning area, respectively.

TABLE II
Summary of the Surface Analysis from the AFM Topography Images (50 × 50 μm^2)

Type of rubber	Average roughness (nm)	Root-mean-square roughness (nm)	Average height (nm)	Average diameter (μm)		Average cavity depth		Sample appearance
				D_w	D_N	$(d/R)_w$	$(d/R)_N$	
HTBD	118 ± 2	153 ± 3	735 ± 75	1.2 ± 0.12	1.2 ± 0.11	0.84 ± 0.03	0.82 ± 0.03	Opaque
LEBD	29 ± 2	38 ± 3	202 ± 5	0.54 ± 0.08	0.40 ± 0.07	0.59 ± 0.05	0.56 ± 0.05	Translucent
HEBD	13 ± 1	16 ± 1	111 ± 21	N/A		N/A		Transparent

Average roughness, given by the average deviation of the data, refers to the average of the data within the area; root-mean-square roughness is given by the standard deviation of the data; average height is given by the average height of the area.

be performed to ensure that the spherical domains are indeed composed of rubber instead of an empty hole which is surrounded by resin. Figure 6 collects the plots of approaching force–distance curves of the matrix and the dispersed domain as a function of applied load. The measurements were carried out at room temperature, which falls in between the T_gs of the two components. Thus, at this testing temperature, the probe is expected to indent the rubbery domain much more than it does to the matrix phase. At the lowest external applied load, the probe indented the matrix and the rubbery domain 100 and 145 nm, respectively. As higher external loads were applied to the cantilever, a greater indentation depth was observed. This phenomenon has been reported by earlier researchers[25] and can be used to identify a multiphase system bearing components with different thermal (T_g) and mechanical properties (elastic modulus).

By varying the external force imposed on the cantilever, one can generate a force spectrum of indent stiffness, normal force normalized to the indentation depth, as a function of external loads, which is illustrated in Figure 7. As the matrix phase is less deformable than the flexible rubbery domain, the material response of the former appears to be more sensitive. Figure 7 illustrates this point by showing that the indent stiffness increases more rapidly for the matrix than for the dispersed phase upon increasing the external load. Furthermore, the matrix exhibits greater contact stiffness than the dispersed phase in the whole force range studied, which serves as strong evidence to support the distinguished features of these two phases.

Investigation on the dispersed phase

Particle size and its distribution

It has been well documented that the particle size distribution is of crucial importance in achieving a high toughening efficiency.[26] According to an earlier publication,[3] rubbery domains with an average diameter in the range of 0.1 and 3 μm are the most effective size for toughening. Thus, a quantitative particle analysis is necessary, as it can be used to predict or support the mechanical data. Shown in Figure 8 are the histograms of particle diameter for the polybenzoxazine resins modified with 10 wt % HTBD and LEBD,

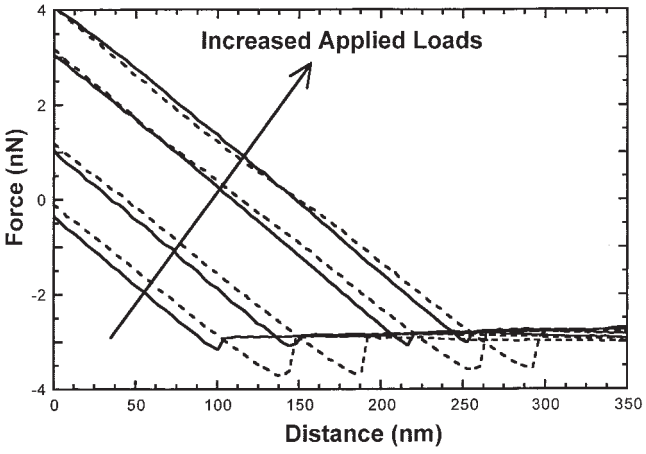

Figure 6 Force–distance curve (F–d) measurements on the polybenzoxazine resin modified with 10 wt % HTBD rubber. Solid line and dash line represent the matrix phase and the dispersed phase, respectively.

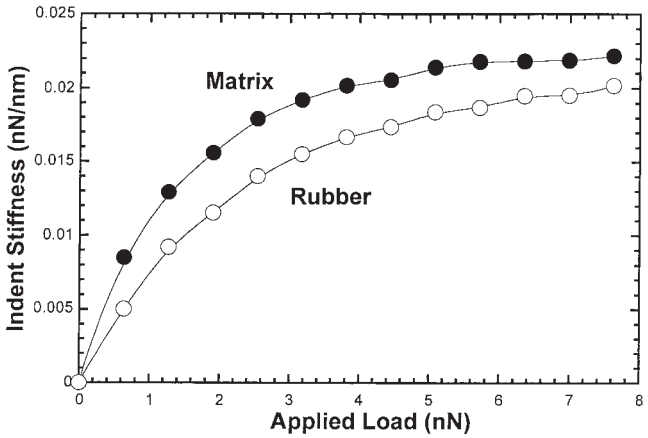

Figure 7 Indent stiffness of the matrix and the dispersed phase in the polybenzoxazine resin modified with 10 wt % of HTBD, as a function of externally applied loads.

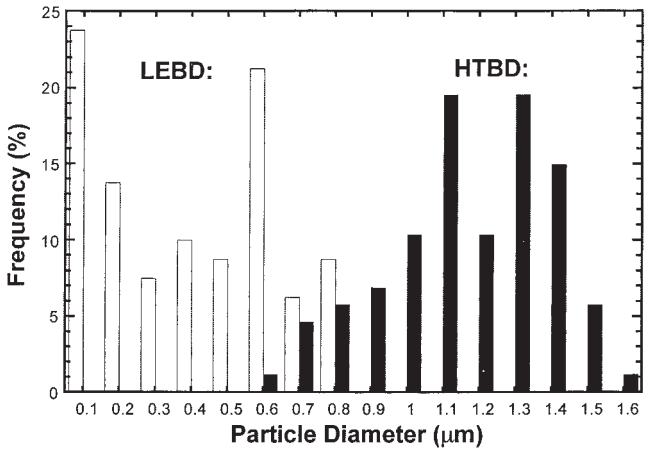

Figure 8 Quantitative particle analysis of the polybenzoxazine resins blended with 10 wt % of HTBD and LEBD rubber.

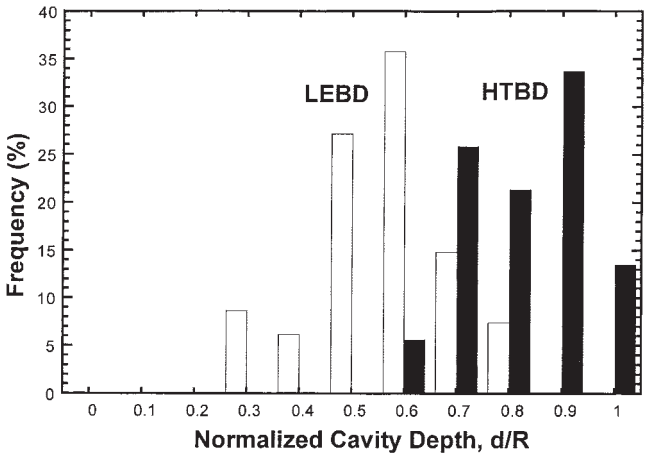

Figure 9 Quantitative cavity depth analysis on the polybenzoxazine resins blended with 10 wt % of HTBD and LEBD rubber, respectively.

respectively, while the calculated number, D_N, and weight–average diameter, D_w, are listed in Table II. The LEBD blend yielded a smaller number–average diameter of 0.40 ± 0.07 μm than the did HTBD system (1.2 ± 0.11 μm), indicating a more compatibilized blend morphology. From these data, it can be interpreted that the functional group from the LEBD rubber serves to minimize the surface tension at the interphase[3] and, subsequently prevents the rubber from segregating to large domains upon thermal curing. This type of epoxidized rubber has also been used to toughen epoxy resins,[11,27,28] and the size of the domain varied with the reactivity in a similar fashion as observed in our system. The average particle diameter of the LEBD and the HEBD modified epoxy resin was reported to be 2.3 ± 0.5 and 0.33 ± 0.09 μm, respectively.[27,28]

Cavity depth and its distribution

The normalized cavity depth, d/R, reflects the amount of rubber remaining after fracture. A d/R that is close to 0 would indicate a strong interphase bonding. Figure 9 depicts the histograms of d/R for resins modified with HTBD and LEBD rubber, respectively, and the average values are listed in Table II. A higher number–average d/R of 0.82 ± 0.03 was estimated in the HTBD blend wherein a weak interphase adhesion was expected, and a lower value of 0.56 ± 0.05 was obtained in the LEBD system wherein strong matrix-rubber bonding should appear. The acquired data has confirmed that when nonreactive HTBD was used, the primary interphase bonding, which involves only weak van del Waals forces, would not be sufficient to transfer the stress across the boundary. As a consequence, HTBD rubber is detached from the adjacent matrix upon fracture, which accounts for the appearance of a deeper cavity. Reactive LEBD, however, reinforces the interphase strength by chemical reaction, and thus, the particle can accommodate a substantial amount of elastic energy via elongation before failure occurs, resulting in mildly cavitated domains.

Correlation between particle size and cavity depth

The particle size and its distribution within rubber-toughened thermosets have been studied extensively in the past, yet a correlation between the particle diameters and the degree of internal rubber cavitation is yet to be established. For this purpose, Figure 10 collects the plots of normalized cavity depth as a function of particle diameter for the resin modified with HTBD and LEBD rubber, respectively. Interestingly, it was found that the degree of cavitation appeared to be greater as the particle diameter increased in the LEBD

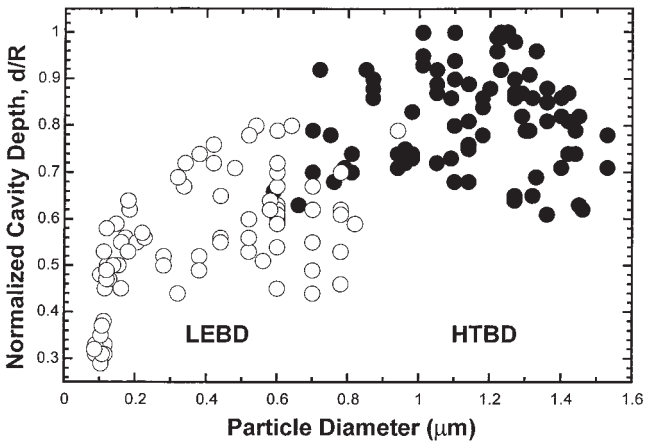

Figure 10 Correlation between particle diameter (D) and normalized cavity depth (d/R) on the polybenzoxazine resins blended with 10 wt % of HTBD and LEBD rubber.

system; yet the cavity depth in the HTBD blend did not seem to be sensitive to the particle diameter. This can be explained by two factors. First, only one type of interphase bonding existed in the HTBD blend which, was the weak van del Waals interaction and, second, the interphase thickness in the same blend system should remain identical regardless of particle size. Hence, the consistent thickness and strength of the interphase in all dispersed domains of the HTBD system would ensure a similar degree of cavitation. However, a mixture of weak physical interaction and strong chemical bonding should coexist in the LEBD system because of the presence of the reactive epoxy moiety on the rubber backbone. Small particles, composed of rubber with grafted resins, should possess a stronger or a more diffused interphase; yet, large ones, segregated from the nonreactive portion, retain only weak van del Waals forces across a sharp interphase. In conclusion, the particle-size dependence of the cavity depth observed in the HTBD is due in part to the mixture of two types of interphases.

Attention should also be drawn to some other possibilities that might account for the less intense cavitation seen in small spheres as compared with the large ones. For instance, large particles often trigger the crack formation in the early stage of the fracture process, owing to the capability of bearing a large stress concentration before breakage. Cracks initiated would be propagated along the nearest rubbery domain to dissipate as much energy as possible by connecting small inclusions together and would be terminated upon the completion of energy release. In other words, large particles, which act as crack initiators, are more likely to be completely detached from the interphase than are small ones, which only serve as passive crack propagators. Accordingly, in addition to a weak interphase strength as interpreted in the previous section, a larger particle size in the HTBD blend also accounts for the observed greater cavity depth than that in the LEBD.

Bulk viscoelastic properties studied by DMA

The effect of rubber addition on the viscoelastic properties or relaxation behavior of the glassy polybenzoxazine resin at various temperatures was investigated by DMA and is discussed in the following sections.

Loss modulus (g'') and relative loss factor (tan δ)/(tan $\delta)_0$

Depicted in Figure 11(a) is the loss modulus (G″) plotted against temperature. Three thermal relaxation processes, α, β, and γ, from high temperature to low temperature are discussed. The first G″ peak, α-relaxation, which is located at the highest temperature of 113°C, denotes the glass transition (T_g) of this particular resin. The second G″ peak, β-relaxation, centered at 5°C, provides information on the homogeneity of the network structure and the amount of uncrosslink segments.[29] The T_g of the phase-separated HEBD rubber was found to be at −25°C. Third, the γ-relaxation, roughly positioned at −65°C, is from the in-chain segmental motion of the long chain amine between benzoxazine backbones.[16] Two sharp peaks in the low temperature region centered at −77 and −54°C can be assigned as the T_g of the phase-separated HTBD and LEBD rubber, respectively. Despite the fact that the rubber T_g coincides with the γ-relaxation of the resin, the magnitude of the former is significantly greater when compared with a weak energy dissipation event that occurred at such a low temperature. Since no apparent chemical interaction in the molecular level should exist between the long chain amine moiety and the rubber, the γ-relaxation appeared to be intact upon blending, which was anticipated.

The fact that T_g of the phase-separated HEBD rubber may have overlapped with the β- relaxation of the resin, as indicated by a broad transition, has made the assignment difficult. To distinguish the rubber transition from the resin relaxation, one can plot the relative damping factor, which is the ratio of tan δ (blend) to tan δ_0 (neat resin), against temperature, as depicted in Figure 11(b)**.** This quantity can be used as an energy dissipation index to measure the extra energy being released by the incorporation of rubber. A value close to unity is indicative of a damping property similar to the neat resin. Three peaks in the low temperature region, centered at −75, −50, and −25°C, are in accordance with the T_g of the phase- separated rubber estimated previously from the G″ peak. Moreover, the three maxima in the high temperature region, located at 80, 72, and 70°C, signify the T_g of the continuous resin. An increased energy dissipation by about 80 and 50% at the rubber T_g was found in the HTBD and LEBD blend, respectively, and only 10% was noticed in the HEBD system. The data reinforce our previous morphological observation by showing that the HTBD blend, wherein larger rubber segregations appeared, dissipated a much greater amount of energy than did the LEBD and HEBD systems, wherein finer and fewer particles were found. Blends with a larger and greater number of rubbery domains can accommodate, as well as release elastic energy by deforming the particles, resulting in an improved toughness. In addition, the relative damping factor detected at the matrix T_g is found to increase with rubber reactivity, as more incorporated rubber can facilitate the energy dissipation by plastically yielding the softened matrix.

Shifting of glass transition temperatures (δt_g)

The difference between the T_g of the two components before blending, ΔT_g (neat), was calculated from the

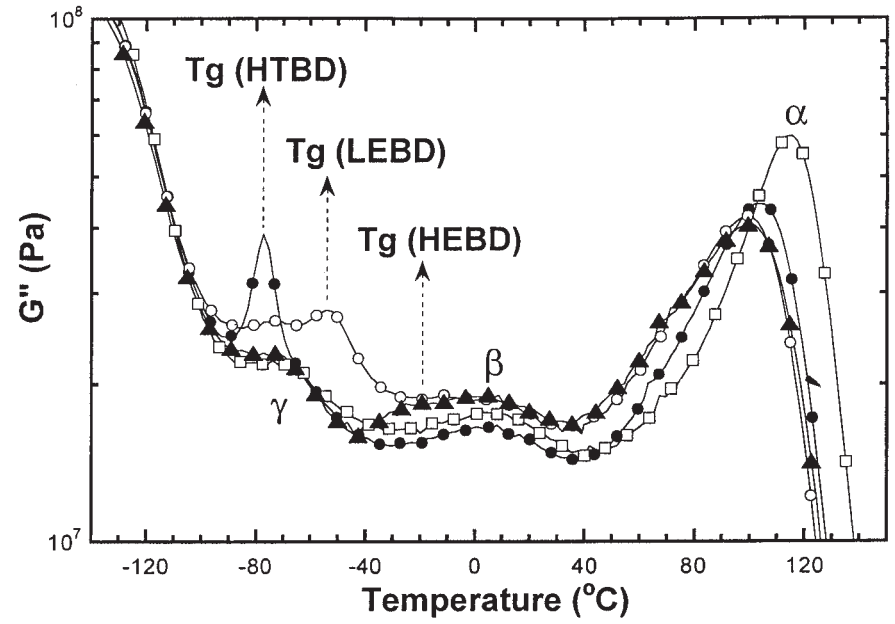

(a) Loss Modulus (G"):

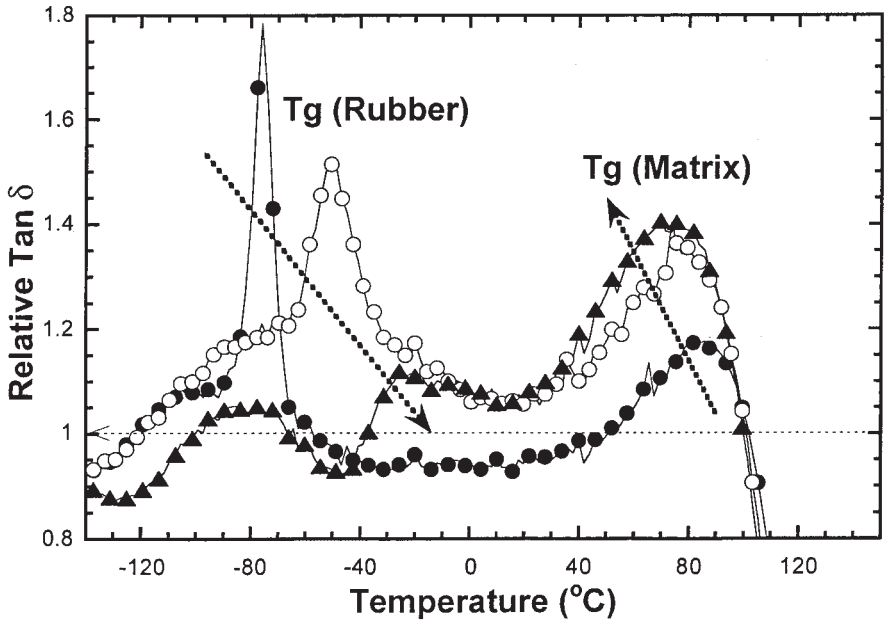

(b) Relative Loss Factor (G"):

Figure 11 (a) Loss modulus (G″) of neat polybenzoxazine resin (□) and its blends modified with 10 wt % of HTBD (●), LEBD (○), and HEBD (▲) rubber, respectively. (b) Relative loss factor, (tan δ)/(tan δ)$_0$, of polybenzoxazine resins modified with 10 wt % of HTBD (●), LEBD (○), and HEBD (▲) rubber, respectively.

T_g of pure rubber and the neat resin. The T_g difference between two components upon blending, ΔT_g (blend), was determined from the G″ peak of the matrix and dispersed phase in the DMA spectra. Both of these values can be found in Table III. It is inferred that this quantity, ΔT_g (blend), denoting the strength of interaction between the two blend components in the molecular level, can be used to indicate the blend compatibility. A considerable shifting of T_g, suggesting a high compatibility, was observed in the HEBD system, which is in agreement with the AFM images illustrated in the early section. No detectable signs of phase separation were found in the images, reflecting a significantly high miscibility between the polybenzoxazine resin and the HEBD rubber. However, very little T_g shifting was shown in the HTBD system, suggesting a low blend compatibility. This result is again in accordance with the AFM images displayed

TABLE III
Thermal Transitions of the Rubber-Modified Polybenzoxazine Blends Estimated from Loss Modulus (*G*") Peak Values in the DMA Spectra

Blends	T_g (Resin) α (°C)	T_g (Rubber; °C)	ΔT_g (Blend; °C)	ΔT_g (Neat; °C)	FWHH of α (°C) (Tan δ)	Dissolved/Phase-separated rubber (wt %)
Neat resin	114	N/A	N/A	N/A	59	0/0
HTBD	103	−77	180	189	64	3/7
LEBD	99	−54	153	174	67	5/5
HEBD	99	−25	124	161	71	6/4

ΔT_g (neat) was computed from the T_g difference between the neat resin and the original rubber modifier prior to blending. ΔT_g (blend) was determined from the difference between the T_g of matrix phase and that of the dispersed rubber phase in the blend system.

previously, in which rubber segregated domains as large as 3 μm in diameter were detected.

Amount of dissolved and phase-separated rubber

In rubber toughening, it was known that the rubber dissolved homogeneously into the continuous phase, contributing to a significant matrix T_g reduction, acts as softeners and facilitates the shear yielding of the glassy resin. They play a critical part in the late stage of fracture process. Phase-separated rubber, which functions as a stress concentrator or crack initiator, is most responsible for the enhanced fracture toughness.[11] The presence of discrete particles with fairly large sizes has a profound influence on the early stage of the fracture process. Accordingly, it is necessary to estimate the amount of dissolved rubber not only for an accurate morphological interpretation but also to separate two distinct toughening mechanisms from each other. The amount of dissolved rubber was calculated from the Fox equation under the assumption that only the dissolved rubber contributed to the matrix T_g depression.[30] T_g of neat resin and its blends were estimated from the G" peak in the DMA spectrum, and T_g of the pure rubber were adopted from the literature value, which was also determined by DMA.[11] The weight percentage of dissolved HTBD and LEBD rubbers in the polybenzoxazine matrix as well as that of the phase-separated rubber is listed in Table III. It can be seen that the dissolved rubber increased with the epoxy content or the rubber reactivity. Once again, these data corroborate fairly well with the surface phenomena probed by AFM, where it was found that the majority of highly reactive HEBD was dissolved thoroughly in the resin and did not appear to be experimentally distinguishable from the continuous phase.

If we correlate the calculated values from this section with Figure 11(b), it can be found that, for the resin blended with 10 wt % HTBD rubber, 80% of the extra damping observed at the rubber T_g is attributed to 7% of phase-separated rubber, yet only 40% of the extra damping detected at the matrix T_g is derived from 3% of dissolved rubber. Thus, it seems that both of the dissolved and phase-separated rubber can facilitate the energy dissipation upon mechanical deformation in high and low temperature region, respectively, yet the latter appears to be much more effective.

Elastic modulus (g')

Since rubber modifier has a low T_g and a relatively low modulus, the effect of this soft inclusion on the mechanical properties at various temperatures is of interest. One can measure the softening effect by relative modulus (RM), which is derived by normalizing the blend modulus (G′) over the modulus of the neat resin (G'_0). This is illustrated in Figure 12, where the relative elastic modulus (G'/G'_0) of various rubber-modified polybenzoxazines is plotted against temperature. Below -90°C, RM close to unity was detected regardless of the types of the rubber modifiers being used, inferring that the "softening effect" cannot be visualized at such a low temperature when the whole

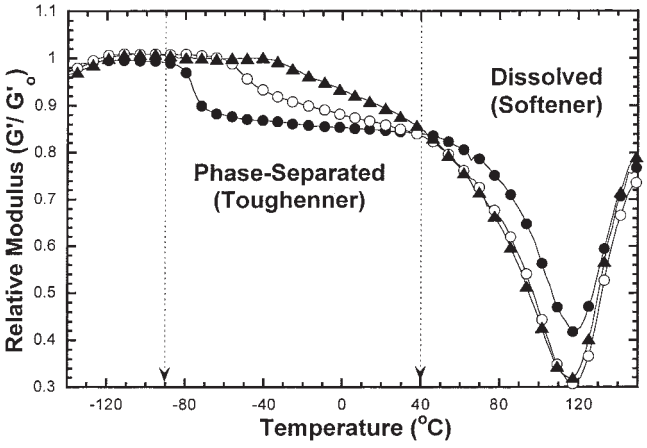

Figure 12 Relative modulus (G'/G'_0) of polybenzoxazine resins modified with 10 wt % of HTBD (●), LEBD (○), and HEBD (▲) rubber, respectively.

specimen, including the soft inclusion, were frozen. The onset temperature of the softening effect located at −90, −65, and −40°C, for HTBD, LEBD, and HEBD system, respectively, can be noticed. This phenomenon can be associated with the T_g of the rubber modifier, centered at several ten degrees higher, as listed in Table III. The overall modulus reduction of roughly 15% in the temperature range between −90 and 40°C is attributed to the softening behavior of the dispersed rubber phases. On the other hand, the drastic modulus reduction of up to 70% at temperatures above 40°C is related to the softening of the continuous matrix. The HTBD blend yielded a greater RM in this temperature range, which is attributed to a slightly lower amount of dissolved rubber in the resin, as compared with the LEBD and HEBD systems.

CONCLUSIONS

Three types of HTBD rubber with various epoxy contents are utilized as reactive modifiers for the polybenzoxazine resin in this study. Phase-separated domains with an average diameter of 1.2 ± 0.12 μm are revealed in the resin modified with nonepoxidized HTBD, and a very rough fracture surface with numerous shear bands appears upon fracture. Dispersed domains with an average diameter of 0.54 ± 0.08 μm occur in the resin modified with LEBD rubber (low epoxy content), yet no distinguishable phase separation is noticed in the blend incorporated with HEBD rubber (high epoxy content). The higher the epoxy concentration in the rubber is, the more compatible the morphology appears and the smoother the surface is revealed, indicating a fairly brittle failure.

Reactive modifier, such as LEBD in this case, reinforces the strength of interphase by chemical reaction, resulting in a relatively mild degree of rubber cavitation upon fracture. When nonreactive rubber such as HTBD is used, the weak interphase, where only a weak van del Waals force exists, is not strong enough to transfer the stress across the boundary. In this case, an adhesive failure occurs at the interphase and a greater amount of debonded rubber is revealed after fracture. The extent of rubber cavitation corresponds well with the particle diameter. Large particles cavitate more intensively than do the small ones, implying a sever interphase rupture or an adhesive failure.

Bulk viscoelastic properties evaluated by DMA corroborate fairly well with the surface phenomena probed by AFM. Matrix T_g reduction and rubber T_g increment appear to be the greatest (37°C) when HEBD rubber is incorporated into benzoxazine resin, confirming a high strength of interaction on the molecular level. On the other hand, the least compatible HTBD system exhibits only a total T_g shift of 9°C. The majority of the HEBD rubber is dissolved homogeneously into the benzoxazine resin as estimated from Fox equation and nearly no dispersed rubber domains are experimentally distinguishable from the continuous phase as indicated in the AFM images. Both of the dissolved and phase-separated rubber can facilitate the energy dissipation upon mechanical deformation, yet the latter appears to be much more effective, as only 40% of extra damping is observed from the former compared with 80% from the latter.

References

1. Ishida, H.; Lee, Y.-H. Polymer 2001, 42, 6971.
2. Ishida, H.; Lee, Y.-H. Polym Polym Compos 2001, 9, 121.
3. Verchere, D.; Sautereau, H.; Pascault, J.-P.; Moschiar, S. M.; Riccardi, C. C.; William, R. J. J. Toughened Plastics, I; Riew, C. K., Kinloch, A. J., Eds.; ACS: Washington DC, 1993; p 335.
4. Ishida, H.; Allen, D. J. J Polym Sci Phys Ed 1996, 34, 1019.
5. Kinloch, A. J. Rubber-Toughened Plastics; Riew, C. K., Ed.; ACS: Washington, DC, 1989; p 67.
6. Huang, Y.; Hunston, D. L.; Kinloch, A. J.; Riew, C. K. Toughened Plastics, I; Riew, C. K., Kinloch, A. J., Ed.; ACS: Washington, DC, 1993; p 2.
7. Pearson, R. A.; Yee, A. F. J Mater Sci 1986, 21, 2475.
8. Kinloch, A. J.; Shaw, S. J.; Hunston, D. L. Polymer 1983, 24, 1355.
9. Kinloch, A. J.; Shaw, S. J.; Tod, D. A.; Hunston, D. L. Polymer 1983, 24, 1341.
10. Kang, B. U.; Jho, J. Y.; Kim, J.; Lee, S. S.; Park, M.; Lim, S.; Choe, C. R. J Appl Polym Sci 2001, 79, 38.
11. Bussi, P.; Ishida, H. Polymer 1994, 35, 956.
12. Jang, J.; Seo, D. J Appl Polym Sci 1998, 67, 1.
13. Shaffer, O. L.; Bagheri, R.; Qian, J. Y.; Diamonie, V.; Pearson, R. A.; El-Aasser, M. S. J Appl Polym Sci 1995, 58, 465.
14. Mathur, D.; Nauman, E. B. J Appl Polym Sci 1999, 72, 1151.
15. Chen, T.; Bai, Y.; Sun, R. J Appl Polym Sci 1998, 67, 569.
16. Allen, D. J.; Ishida, H. J Appl Polym Sci, in press.
17. Paiva, A.; Sheller, N.; Foster, M. D.; Crosby, A. J.; Shull, K. R. Macromolecules 2000, 33, 1878.
18. Beake, B. D.; Leggett, G. J.; Shipway, P. H. Surf Interface Anal 1999, 27, 1084.
19. Beake, B. D.; Ling, J. S. G.; Leggett, G. J. J Mater Chem 1998, 8, 2845.
20. Gibson, C. T.; Watson, G. S.; Myhra, S. Wear 1997, 213, 72.
21. Eaton, P. T.; Graham, P.; Smith, J. R.; Smart, J. D.; Nevell, T. G.; Tsibouklis, J. Langmuir 2000, 16, 7887.
22. Gauthier, S.; Aime, J. P.; Bouhacina, T.; Attias, A. J.; Desbat, B. Langmuir 1996, 12, 5126.
23. Ning, X.; Ishida, H. J Polym Sci Polym Phys Ed 1994, 32, 921.
24. Rowe, E. H.; Riew, C. K. Plast Eng 1975, 31, 45.
25. Syed Asif, S. A.; Wahl, K. J.; Colton, R. J.; Warren, O. L. J Appl Phys 2001, 90, 1192.
26. van der Wal, A.; Verheul, A. J. J.; Gayman, R. J. Polymer 1999, 40, 6057.
27. Bussi, P.; Ishida, H. J Polym Sci Phys Ed 1994, 32, 647.
28. Bussi, P.; Ishida, H. J Appl Polym Sci 1994, 53, 441.
29. Ning, X.; Ishida, H. J Polym Sci Phys Ed 1994, 32, 921.
30. Fox, T. G. Bull Am Phys Soc 1956, 1, 123.